Int. J. Heat Mass Transfer. Vol. 29, No. 9, pp. 1383–1392, 1986
Printed in Great Britain

0017–9310/86 $3.00 + 0.00
Pergamon Journals Ltd.

The stability of vertical thermal buoyancy induced flows in cold pure and saline water

Z. H. QURESHI
Department of Mechanical Engineering, The Johns Hopkins University, Baltimore, U.S.A.

and

B. GEBHART
Department of Mechanical Engineering and Applied Mechanics, University of Pennsylvania, Philadelphia, U.S.A.

(*Received* 25 *July* 1985 *and in final form* 21 *January* 1986)

Abstract—Buoyancy driven flows in cold pure and saline water very commonly arise. The anomalous density behavior of cold water, for example, a density extremum at about 4°C in pure water at atmospheric pressure, commonly has very large effects on flow and transport. Resulting mechanisms have been studied for various geometries and conditions, primarily for laminar flow. This study assesses the stability and instability mechanisms of developing flows adjacent to a vertical surface subject to both uniform flux and isothermal bounding conditions, in pure water at two pressure levels. The specific condition treated is that in which the quiescent ambient medium is at the density extremum condition. It is found that even this relatively weak effect, the variation to a density extremum across the thermal layer in the fluid, has important effects on instability and disturbance growth downstream. However, the nature of the instabilities and their selective amplification are similar to those well known for more ordinary fluid conditions. The new results here are compared with recent measurements of disturbance behavior, with excellent agreement.

1. INTRODUCTION

THE PHENOMENA of instability, disturbance growth and transition in buoyancy induced boundary layers are very important in applications. They have been investigated analytically, numerically and experimentally. Most of the studies pertain to isothermal or uniform flux conditions at a vertical surface in air or water. Instability arises in a laminar flow when a balance of buoyancy, pressure and viscous forces contributes net energy to disturbances, causing their amplification as they are convected downstream.

Such instability characteristics are modified if the fluid state is near the condition of a density extremum. This occurs in pure water at about 4°C at atmospheric pressure. The temperature at maximum density, $t_m(s,p)$, is known to decrease both with increasing water salinity and pressure level. A wide range of temperature, salinity and pressure levels occurs both in terrestrial waters and in technological processes and these effects are often very important.

Almost all past stability analyses have used the Boussinesq approximation. That is, the local density difference $(\rho_r-\rho)$ is approximated linearly in terms of temperature and/or concentration differences, $(t-t_r)$ and $(s-s_r)$. The respective volumetric coefficients of expansion are taken as constants. This approximation results in the local instantaneous buoyancy force, $g(\rho_r-\rho)$, becoming $g\beta_t(t-t_\infty)$, for thermal effects alone, where t_∞ is the temperature of the ambient.

Analysis and calculation of instability then proceeds from the force-momentum and energy equations, written in terms of local average flow quantities and disturbance effects on velocity, pressure, density and temperature. The equations are then linearized in disturbance amplitude. Several other often reasonable approximations are also made. The results are a force-momentum and an energy equation, in terms of local disturbance amplitudes, superimposed on a steady boundary region base flow. For buoyant flows, these equations are coupled by the temperature disturbance buoyancy force in the force-momentum equation.

Assuming the form of both the streamwise and temporal disturbance behavior, these equations have been solved for many kinds of vertical and inclined buoyancy driven and mixed convection flows. The matters of principal interest have been: the downstream location of incipient instability, in terms usually of local Grashof number; the downstream growth rate of disturbance amplitude, beyond that location; and the variation of disturbance amplitude across the boundary region. These all depend on the heating condition, on the geometry of the flow and on the Prandtl number.

Many experiments have shown that such analysis and calculation frequently very accurately predict the actual instability and disturbance growth characteristics which result in the first local turbulence. This turbulence, in turn, initiates a downstream transition region to full turbulence. A thorough recent review of the status of this field is given in Ref. [1]. This review also summarizes improved methods of formulation and analysis, as well as information from experiments

NOMENCLATURE

A disturbance amplitude ratio, equation (21)
$b(x)$ and $c(x)$ similarity functions
B characteristic frequency for an isothermal surface condition
B^* characteristic frequency for a uniform flux surface condition
B_2, B_3 constants
c wave speed, m/s
c_p specific heat, J/kg °C
$d(x)$ temperature function, °C
$f = f(\eta)$ generalized stream function
f physical frequency
g gravitational force, m/s^2
Gr_x local Grashof number
k thermal conductivity, W/m °C
n power law exponent
N power law coefficient
p pressure, bar
Pr Prandtl number
$q = q(s,p)$ exponent in the density equation
$q''(x)$ local surface heat flux, W/m^2
s salinity, ‰ (ppt)
$S(\eta)$ disturbance temperature amplitude function
t temperature, °C
t' disturbance temperature
U_c characteristic velocity, m/s
u, v velocity components, m/s
$u'v'$ disturbance velocity components
x, y, z coordinates.

Greek symbols
$\alpha = \alpha(s,p)$ temperature coefficient in the density equation, 1/°C
α_i disturbance amplification rate
α_r disturbance wave number
β_t thermal expansion coefficient, 1/°C
β disturbance frequency
δ boundary layer thickness
λ wave length, m
$\eta = \eta(x,y)$ similarity variable
ν kinematic viscosity, m^2/s
$\rho = \rho(t,s,p)$ density of water, kg/m^3
Φ disturbance velocity amplitude function
ϕ generalized temperature
$\psi = \psi(x,y)$ stream function
$\psi' = \psi'(x,y,\tau)$ disturbance stream function
τ time.

Subscripts
i imaginary part of eigenvalues and eigenfunctions
il ice–liquid interface
m extremum condition
o at the fluid–solid interface
r reference, real part of eigenvalues and eigenfunctions
∞ unstratified quiescent ambient medium.

on the progression of turbulence production, the nature of the developing turbulence and the indicated predictive parameters which bound the transition region.

The present results concern the instability and disturbance growth characteristic in vertical thermally driven flows in cold water. The buoyancy force may not then be generally approximated linearly, in terms of temperature. Figure 1 indicates the density variation with temperature, $\rho(t,s,p)$, at salinity levels of $s = 0$, 20 and 35 ppt, at a pressure of 1 bar, and also for $s = 20$ ppt, at 10 and 20 bars. Clearly, a linear approximation is not generally appropriate, over any considerable range of temperature. An even greater anomaly arises when the surface and ambient temperatures, t_o and t_∞, span the extremum. This is most apparent in relation to the bottom curve. Then a large buoyancy force reversal arises across the thermal boundary layer. This introduces additional mechanisms toward instability, arising from the tendencies to bi-directional boundary region flow.

Such tendencies, toward bi-directional and flow

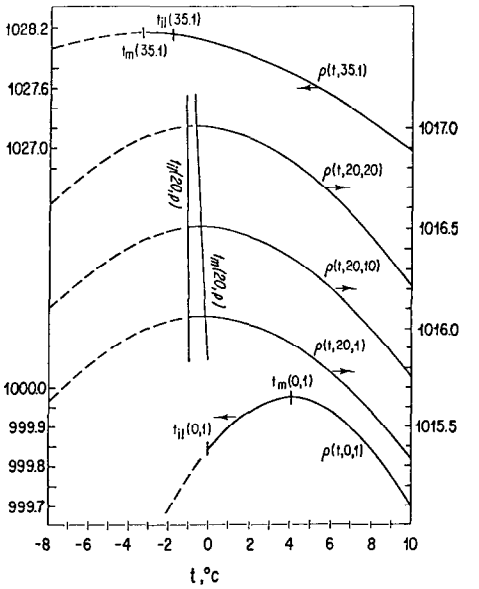

FIG. 1. The density-temperature dependence at various s and p, in kg m^{-3}. Both t_m and t_{il} are shown.

reversal effects, have had considerable attention, mostly in most recent years. The severity and occurrence of changed flow patterns are sometimes best correlated in the following temperature parameter.

$$R = \frac{t_m(s,p) - t_\infty}{t_o - t_\infty}. \tag{1}$$

This parameter places the imposed conditions, t_o and t_∞, with respect to the extremum condition t_m. Upflow arises for $R \leqslant 0$, $R \geqslant 1/2$ is downflow. Local buoyancy force reversals arise across the range of $0 < R < 1/2$.

Given the importance of cold water flows, there have been many experiments and calculations to assess the transport arising under the conditions of the reduced level of buoyancy and the reversals implied in Fig. 1. A full summary of the results is given in Refs. [2] and [3], along with measured and calculated transport information for vertical plane flows. Studies [4] and [5] probe the nature of transport response in the region of buoyancy force reversal, $0 < R < 1/2$. These collective studies show that many complicated transport regimes arise. Some are not of boundary region form, as shown in Ref. [6]. With saline diffusion effects added, as in Refs. [7] and [8], a very large diversity of additional effects and regimes also arise. Under some conditions ordinary transition occurs. Under others, laminar and turbulent regions co-exist or develop independently in different regions.

Very little is known about how some of these flows are actually generated and driven. This paper considers an early aspect of such flows, how laminar instability arises and progresses to disturbance amplification downstream, in a vertical thermally driven flow.

The two studies to date concerning instability, in external vertical flows, are those in Refs. [9] and [10]. They concern an isothermal surface, at t_o, in an unstratified quiescent ambient, at t_∞. In Ref. [9], the effects of a tendency toward a density extremum, on neutral stability, are determined. This includes the regimes in the regions $R < 0$ and $R > 1/2$. Then, no buoyancy force reversal arises. It was shown that the evaluation of the buoyancy force, accurately accounting for the tendency to a density extremum, results in enhanced downstream stability.

The experiments, in Ref. [10], at $R = 0$, 0.1 and 0.4, entered the gap of buoyancy force reversal, $0 < R < 1/2$, on each side. Downstream instability and processes early in transition were studied. The data indicated the same kind of selective amplification mechanism long known to be operative with ordinary fluid behavior. Transition again followed from such disturbances. Both disturbance growth and transition were delayed, by the reduced buoyancy force, as predicted by calculations.

The present study follows on these results. Detailed instability calculations were made for both the uniform surface heat flux, q'', and uniform surface temperature, t_o, bounding conditions. The results first show the effect of the tendency to an extremum on initial instability. Then, detailed downstream disturbance growth characteristics are given and compared with those in ordinary fluids. For all calculations, the ambient temperature, t_∞, is taken as t_m. That is, $R = 0$. Finally, the uniform flux disturbance growth predictions are compared with the data in Ref. [11], concerning actual disturbance behavior.

The following sections formulate the basic laminar flow, for both bounding conditions, then the disturbances. The instability equations are then given. The numerical procedure is then set forth and disturbance amplitudes and stability planes are given. The subsequent comparison with limited data shows very good agreement.

2. THE BASIC BOUNDARY REGION FLOWS

The density variations in Fig. 1 indicate that the rate of density changes are very small around the extremum. Therefore, it is necessary to calculate the density, $\rho(t,s,p)$ from a very accurate equation of state. Past equations are very complicated. They would result in a very large number of circumstance-dependent parameters in the formulation. This led to the development, in Ref. [12], of a very much simpler yet very accurate relation. Using this relation, similarity solutions were found in Ref. [3], for two-dimensional boundary layer flows induced by the buoyancy effects of both thermal and saline diffusion.

This density relation will be used here, for both the uniform flux and isothermal vertical surface conditions, in an extensive ambient medium at $t_\infty = t_m/s,p)$, that is, for $R = 0$. Buoyancy is assumed here to arise only from thermal transport. One additional parameter, $q(s,p)$, arises.

The boundary layer equations for two-dimensional plane flow are

$$\frac{\partial u}{\partial x} + \frac{\partial v}{\partial y} = 0 \tag{2}$$

$$\rho\left(u\frac{\partial u}{\partial x} + v\frac{\partial u}{\partial y}\right) = \mu\frac{\partial^2 u}{\partial y^2} + g(\rho_\infty - \rho) \tag{3}$$

$$\rho c_p\left(u\frac{\partial t}{\partial x} + v\frac{\partial t}{\partial y}\right) = k\frac{\partial^2 t}{\partial y^2}. \tag{4}$$

The following transformation is applied, in terms of a similarity variable $\eta(x,y)$, stream function $\phi(x,y)$, or $f(\eta)$, and temperature function, $\phi(\eta)$, as follows:

$$\eta = yb(x), \quad \psi(x,y) = vc(x)f(\eta) \tag{5a}$$

$$\phi(\eta) = \frac{t - t_\infty}{d(x)} \quad \text{where} \quad d(x) = t_o - t_\infty. \tag{5b}$$

The buoyancy force $g(\rho_\infty - \rho)$ in equation (3) is determined from the density relation given below, in which the only temperature effect is $|t - t_m|^q$. This leads

to extremely important simplifications in analysis

$$\rho(t,s,p)=\rho_m(s,p)\{1-\alpha(s,p)[|t-t_m(s,p)|]^{q(s,p)}\}. \quad (6)$$

The functions $\rho_m(s,p)$, $\alpha(s,p)$, $t_m(s,p)$ and $q(s,p)$ apply over a range of salinity, 0 to 40 ppt, at pressure levels to 1000 bars, for the temperature range 0 to 20°C. This equation has an rms accuracy of 10.4 ppm over these ranges. Some typical values of $q(s,p)$ and $\alpha(s,p)$ are listed in Table 1.

For most flows of small physical extent, the effects of pressure on density may be neglected. Therefore, the pressure terms in equation (6) are taken to pertain only to the pressure level. Then the density difference $(\rho_\infty-\rho)$ becomes,

$$\rho_\infty-\rho=\rho(t_\infty,s_\infty,p)-\rho(t,s_\infty,p)$$
$$=\rho_m\alpha|t_o-t_\infty|^q\cdot\phi^q, \quad (7)$$

where $t_m(s_\infty,p)=t_\infty$. Since $\rho_\infty=\rho_m$, the buoyancy force and flow are always up, for t_o on either side of t_∞.

Introducing the transformations (5) and the buoyancy force (7) into equations (2–4), the variations of $b(x)$, $c(x)$ and $d(x)$ are determined to result in similarity. Then η is the similarity variable in the stream and temperature functions, $f(\eta)$ and $\phi(\eta)$. The local Grashof number is conventionally defined as $(gx^3/\nu^2)(\beta_t\Delta t)$, the unit Grashof number times an estimate of the units of buoyancy, $\beta_t(t_o-t_\infty)$. The analogous estimate here is $\alpha|t_o-t_\infty|^q$. With this choice, the transformation, boundary region equations and boundary conditions, for an impervious surface, become

$$Gr_x=(gx^3/\nu^2)\alpha(t_o-t_\infty)^q \quad \text{and} \quad G=4^4\sqrt{Gr_x/4} \quad (8a)$$

$$c(x)=4xb(x)=G \quad \text{and} \quad t_o-t_\infty=d(x)=Nx^n \quad (8b)$$

$$f'''+(3+qn)ff''-(2+2qn)f'^2+\phi^q=0 \quad (8c)$$

$$\phi''+Pr[(3+qn)f\phi'-4nf'\phi]=0 \quad (8d)$$

$$1-\phi(0)=\phi(\infty)=f'(0)=f(0)=f'(\infty)=0, \quad (8e)$$

where η, the characteristic boundary region thickness, δ, and velocity, U_c, are

$$\eta=yG/4x, \quad \delta(x)=4x/G \quad \text{and} \quad U_c(x)=\nu G^2/4x. \quad (9)$$

The above similar solution arises for any reasonable power law variation of $t_o-t_\infty=d(x)=Nx^n$. For an isothermal surface condition, $n=0$ and the equations and boundary conditions reduce to

$$f'''+3ff''-2f'^2+\phi^q=0 \quad (9a)$$

$$\phi''+3Prf\phi'=0 \quad (9b)$$

$$1-\phi(0)=\phi(\infty)=f'(0)=f(0)=f'(\infty)=0. \quad (9c)$$

For a uniform surface heat flux, $n=1/(4+q)$, and the momentum and energy equations and boundary conditions become

$$f'''+\frac{4(3+q)}{(4+q)}ff''-\frac{4(2+q)}{(4+q)}f'^2+\phi^q=0 \quad (10a)$$

$$\phi''+Pr\left[\frac{4(3+q)}{(4+q)}f\phi'-\frac{4}{4+q}f'\phi\right]=0 \quad (10b)$$

$$1-\phi(0)=\phi(\infty)=f'(0)=f(0)=f'(\infty)=0. \quad (10c)$$

The temperature response N is

$$N=\{\sqrt{2\nu q''}/k\sqrt[4]{\alpha g}[-\phi'(0)]\}^{4/(4+q)}.$$

Table 1. Values of $q(s,p)$ at several different pressure and salinity levels

$q(s,p)$	Pressure p (bars)	Salinity s (ppt)	$\alpha(s,p)$
1.0	†	†	β_t
1.5829	1000	0	27.164×10^{-6}
1.8364	1	25.25	10.417×10^{-6}
1.8632	1	35.0	9.381×10^{-6}
1.8948	1	0	9.297×10^{-6}

† $q=1$ represents a linear variation of density with temperature. Then, $\alpha=\beta_t$, the thermal expansion coefficient.

3. THE INSTABILITY FORMULATION

A linear stability analysis is employed. The base flow is assumed subject to the following two dimensional disturbances, in terms of the stream and temperature functions, ψ' and t'.

$$\psi'(x,y,\tau)=U_c\delta\Phi(\eta)e^{i(\hat\alpha x-\hat\beta\tau)} \quad (11a)$$

$$t'(x,y,\tau)=(t_o-t_\infty)S(\eta)e^{i(\hat\alpha x-\hat\beta\tau)}. \quad (11b)$$

Both $\hat\alpha$ and $\hat\beta$ may be complex. Early stability investigations chose $\hat\alpha$ to be real and $\hat\beta$ complex. This formulation predicted the local temporal exponential growth of disturbances. More recent practice has instead considered $\hat\alpha$ complex, with $\hat\beta$ real. This formulation determines the spatial, or downstream, amplification rate.

This is the actual mechanism in a developing boundary region flow and such results have been repeatedly found to be in excellent agreement with experimental results, for many different buoyancy driven flows. See the review in Ref. [1]. The real part of $\hat\alpha$, $\hat\alpha_r=2\pi/\lambda$, is the wave number and $-\hat\alpha_i$ is the spatial (in x) amplification rate. The frequency f is related to $\hat\beta$ as $\hat\beta=2\pi f$. Both $\hat\alpha$ and $\hat\beta$ are generalized, as $\hat\alpha=\alpha\delta$ and $\hat\beta=\beta\delta/U_c$.

The disturbance equations

The instantaneous stream and temperature function, $\psi+\psi'$ and $t+t'$, are substituted into the

complete time dependent flow equations. The usual approximations are applied and the higher order disturbance terms are neglected. The resulting disturbance equations, in similarity form, in terms of disturbance amplitude functions $\Phi(\eta)$ and $S(\eta)$, generalized as shown in equation (11), are

$$\left(f'-\frac{\beta}{\alpha}\right)(\Phi''-\alpha^2\Phi)-f'''\Phi=\frac{1}{i\alpha G}\times[\Phi''''-2\alpha^2\Phi''+\alpha^4\Phi+q(q-1)\phi^{q-2}\times\phi' S+q\phi^{q-1}S'] \quad (12)$$

$$\left(f'-\frac{\beta}{\alpha}\right)S-\phi'\Phi=\frac{1}{i\alpha PrG}(S''-\alpha^2 S). \quad (13)$$

The boundary conditions for a surface of relatively large thermal capacity are

$$\Phi(0)=\Phi'(0)=S(0)=\Phi(\infty)=\Phi'(\infty)=S(\infty)=0. \quad (14)$$

The above equations constitute a sixth order linear ordinary differential equation for the disturbance amplitude distributions $\Phi(\eta)$ and $S(\eta)$. They contain $f(\eta)$ and $\phi(\eta)$, the base flow quantities. The parameters are G, q and Pr and α and β are the eigenvalues. The ratio β/α is the wave speed c.

The effect of anomalous density variation is seen to appear both in the base flow, f and ϕ, as well as in the disturbance momentum equation (12). For temperature conditions very far away from the density extremum, where the Boussinesq approximation is valid, q becomes equal to one. Then the above formulation reduces to the conventional one.

The numerical procedure

The above sixth order linear system was solved numerically, as in Ref. [13], writing the amplitudes Φ and S as

$$\Phi=\Phi_1+B_2\Phi_2+B_3\Phi_3$$
$$S=S_1+B_2S_2+B_3S_3. \quad (15)$$

The subscripts 1, 2, and 3 correspond to the inviscid, the viscous uncoupled and the viscous coupled integrals. For the inviscid limit, the terms of $0(G^{-1})$ may be neglected and the equations (12) and (13) reduce to

$$(f'-c)(\Phi''-\alpha^2\Phi)-f'''\Phi=0=(f'-c)S-\phi'\Phi, \quad \text{where} \quad c=\beta/\alpha. \quad (16)$$

For the remaining linearly independent integrals, the limiting equations for the viscous uncoupled and viscous coupled limits are respectively

$$i\alpha G(f'-c)\Phi''-\Phi''''=0 = i\alpha PrG[(f'-c)S-\phi'\Phi]-S'' \quad (17)$$

and

$$i\alpha G(f'-c)\Phi''-\Phi''''-q(q-1)\phi^{q-2}\phi' S-q\phi^{q-1}S' = 0 = i\alpha PrG[(f'-c)S]-S''. \quad (18)$$

The asymptotic behavior of these integrals, as $\eta\to\infty$, are exponentially decaying and are characterized as

$$\Phi\sim e_1^{-\alpha\eta}, \quad \Phi_2\sim e^{-\alpha_2\eta} \quad \text{and} \quad \Phi_3\sim e^{-\alpha_3\eta}, \quad (19)$$

where

$$\alpha_2=(\alpha^2-ic\alpha G)^{1/2}$$

and

$$\alpha_3=[f_\infty(nq+3)(q-1)Pr+(\alpha^2-ic\alpha PrG)^{1/2}].$$

The corresponding asymptotic behavior of the temperature disturbances is

$$S_1\sim i\alpha PrG\phi'\Phi_1/\{\alpha^2-i\alpha cPrG-[\alpha+(nq+3)Prf_\infty]^2\}$$
$$S_2\sim i\alpha PrG\phi'\Phi_2/\{\alpha^2-i\alpha cPrG-[\alpha_2+(nq+3)Prf_\infty]^2\} \quad (20)$$
$$S_3\sim(\alpha_3^2-\alpha_2^2)(\alpha_3^2-\alpha^2)\Phi_3/\alpha_3.$$

4. NEUTRAL STABILITY CONDITIONS AND DISTURBANCE GROWTH

The above formulation may be used to develop a plane of neutral stability and disturbance growth, for any surface temperature condition $d(x)$ and any set of values of Pr and q. The coordinate of such planes are conventionally $\beta\sim G$. Two kinds of calculations are given here, for both the temperature and the flux surface conditions. The first is for $Pr=11.6$ and $q=1.8948$ and 1.5829. The first value of q is for pure water at 1 bar and the second is for pure water at 1000 bar. An extremum would arise at 1000 bar in subcooled water.

The other calculations, done for comparison, are for a linear dependence of density on temperature, as with the Boussinesq approximation. Then $q=1$. This applies at higher temperature levels and even at lower ones, for very small temperature differences t_o-t_∞. This condition is recovered in the formulation here, in equations (12) and (13) for $q=1$. For these calculations Pr was taken as 11.6, as for cold water, except for some comparisons, when $Pr=6.7$ is used, as at ordinary temperatures.

The tangential velocity, f', and temperature distributions, ϕ, are also calculated. This permits interpretation of instability effects in terms of differing base flows. Disturbance amplitude distributions across the boundary region were also calculated at several downstream locations, various values of G, for comparison with each other and with the data reported in [11], for the flux surface condition.

Neutral stability

For the neutral curve, $\alpha_i=0$ in equations (12) and (13). For a given value of G, a pair of eigenvalues is guessed, i.e. β_r and α_r, and the six integrals Φ_1, Φ_2, Φ_3, S_1, S_2 and S_3 are integrated separately across the boundary region. Using the boundary conditions

$\Phi(0) = S(0) = 0$, B_2 and B_3 are determined from equation (15). The remaining boundary condition $\Phi'(0)$ is satisfied, by adjusting the guessed values of β_r and α_r, until $\Phi'(0)$ is less than 10^{-4}. Each convergence is a neutral point. The neutral curve is generated by obtaining eigenvalues β_r and α_r, over the range of G.

Amplification contours

As a disturbance of a given frequency is convected downstream, from a position G_1 to G_2, the amplitude ratio (A_2/A_1) for the two locations is given by

$$\frac{A_2}{A_1} = \exp\left[-\frac{1}{3+nq}\int_{G_1}^{G_2} \alpha_i \, dG\right] = \exp[A]. \quad (21)$$

The amplification contours, that is, the loci of downstream locations have common values of A, are determined from equation (21). Constant physical frequency paths amount to satisfying the following relations between β and G, for $n = 0$ and $n = 1/(4+q)$, respectively,

$$\beta G^{1/3} = \frac{2\pi f}{\nu}\left[g\alpha(s,p)\frac{(t_o - t_\infty)^q}{\nu^2}\right]^{-2/3} = B \quad (22)$$

and

$$\beta G^{(q+1)/(q+3)} = \frac{32\pi f}{\nu} \times \left[\frac{4^3 g\alpha(s,p)N^q}{\nu^2}\right]^{-(q+4)/2(q+3)} = B^*, \quad (23)$$

where

$$N = \left[\frac{4\nu^2}{g\alpha}\left(\frac{q''}{k[-\phi'(0)]}\right)^4\right]^{1/(q+4)}.$$

Note that B^* and B are constants for a given value of q, frequency f and q'' or $(t_o - t_\infty)$.

To determine the A contours, for given values of $q(s,p)$, Pr and n, the neutral curve is used as the starting point for a particular frequency path. The value of β_r and G at the neutral curve determine B, or B^*, in equations (22) or (23). Then, choosing a value of G further downstream, equations (23) or (24) determines β_r, along the same f path. The complex value of α is guessed, and the calculation is similar to that carried out for the neutral curve. The values of α_r and α_i are corrected to satisfy the boundary condition $\Phi'(0) = 0$, using the Cauchy–Riemann relations $\partial\Phi_r'(0)/\partial\alpha_r = \partial\Phi_i(0)/\partial\alpha_i$, etc., until $\Phi'(0)$ is sufficiently small. The steps of ΔG were typically 5. The values of A are given by equation (21), using the simple trapezoidal rule. This procedure is repeated for a sufficient number of physical frequency paths to determine the constant A contours. An example is seen in Fig. 4, simultaneously for $q = 1.8948$ and 1.0.

Disturbance profiles across the boundary region

These are determined from equation (11). Since the disturbance equations are linear and homogeneous, absolute magnitudes of the disturbances may not be calculated. Therefore, the amplitude distributions are normalized by their maximum values across the boundary region, as follows:

$$\frac{u'}{u'_{max}} = \left[\frac{(\Phi_r')^2 + (\Phi_i')^2}{[(\Phi_r')^2 + (\Phi_i')^2]_{max}}\right]^{1/2} \quad (24)$$

$$\frac{v'}{v'_{max}} = \left[\frac{(\Phi_r)^2 + (\Phi_i)^2}{[(\Phi_r)^2 + (\Phi_i)^2]_{max}}\right]^{1/2} \quad (25)$$

$$\frac{t'}{t'_{max}} = \left[\frac{(S_r)^2 + (S_i)^2}{[(S_r)^2 + (S_i)^2]_{max}}\right]^{1/2}. \quad (26)$$

5. RESULTS

The results for both the uniform flux and isothermal conditions are shown in Figs. 2–6 and 7–11, respectively. In each set, the steady-boundary region profiles, f' and ϕ, are first plotted, for $Pr = 11.6$ and $q = 1.0$, 1.5829 and 1.8948. The heat transfer parameter $[-\phi'(0)]$ is listed in Table 2 for $Pr = 11.6$ and several values $q(s,p)$. In Figs. 3 and 8, neutral stability curves are given. Figures 4 and 9 are the complete stability planes, in terms of downstream disturbance growth A and paths of constant physical frequency, f. The results for both $q = 1.0$ and 1.8948 are given on both figures, for comparison. Finally the normalized disturbance amplitude functions, or u' and t', are given in Figs. 5 and 6, and Figs. 10 and 11.

Downstream amplification

The calculated stability results give both eigenvalues and eigenfunctions. The eigenvalues determine the stability plane. The neutral curve and the region of disturbance amplification are shown, with constant A contours. Most amplified disturbance frequencies are indicated. On the other hand, the eigenfunctions give distributions of disturbance amplitudes, as well as phase angles, across the boundary region.

The uniform flux condition

Figure 2 compares the velocity and temperature distributions for $q = 1.0$, 1.5829 and 1.8948, for $Pr = 11.6$. With increasing values of q, the velocity levels, as f', decrease. However, f' is the physical

Table 2. Values of the heat transfer parameter $[-\phi'(0)]$ for $Pr = 11.6$

	$[-\phi'(0)]$	
$q(s,p)$	Isothermal ($n = 0$)	Uniform heat flux $\left(n = \frac{1}{4+q}\right)$
1.0	1.2200	1.3730
1.5829	1.0971	1.2251
1.8364	1.0557	1.1757
1.8632	1.0517	1.1709
1.8948	1.0470	1.1653

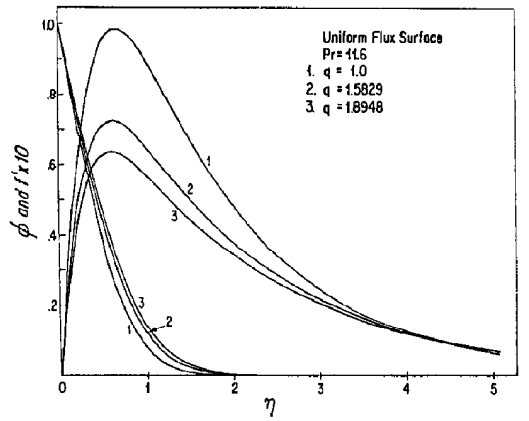

FIG. 2. Distributions of base flow velocity f' and temperature ϕ across the boundary region for a uniform flux surface.

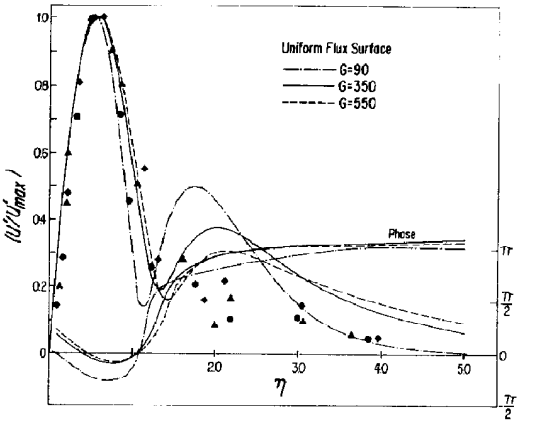

FIG. 5. u'/u'_{max} and phase distributions for a uniform flux surface along a path $B^* = 1.512$, $q = 1.8948$. Experimental data by Qureshi and Gebhart (1981) ● $G = 447$, $x = 53.3$ cm; ▲ $G = 469$, $x = 78.6$ cm; ◆ $G = 606$, $x = 78.6$ cm.

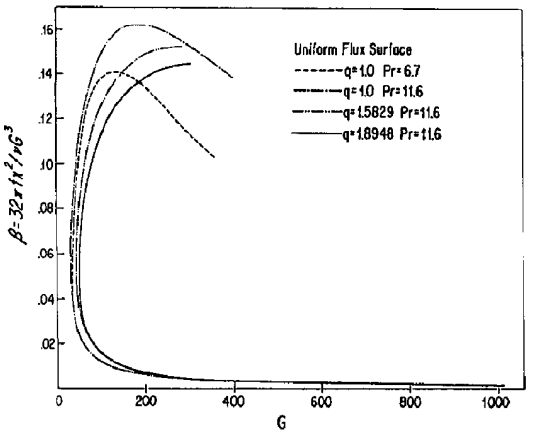

FIG. 3. Neutral stability curves for a uniform flux surface.

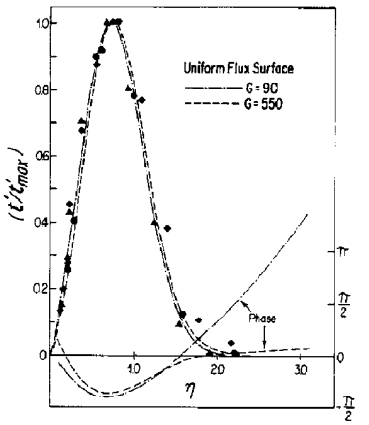

FIG. 6. t'/t'_{max} and phase distributions for a uniform flux surface along a path $B^* = 1.512$, $q = 1.8948$. Experimental data by Qureshi and Gebhart ● $G = 447$, $x = 53.3$ cm; ▲ $G = 469$, $x = 78.6$ cm; ◆ $G = 606$, $x = 78.6$ cm.

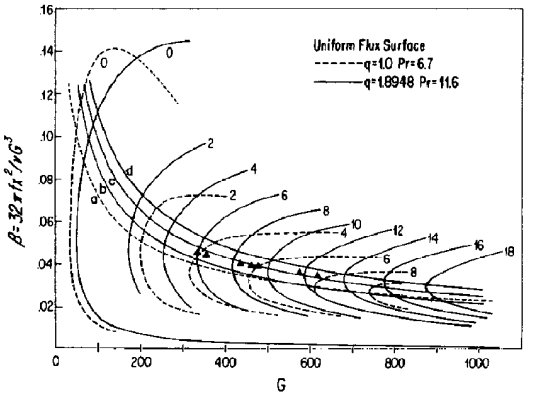

FIG. 4. Amplification rate contours for a uniform flux surface. Curves a, b, c and d represent $B^* = 0.731$, 1.3203, 1.512 and 1.6929, respectively. ▲ Characteristic frequencies in transition observed experimentally by Qureshi and Gebhart (1981).

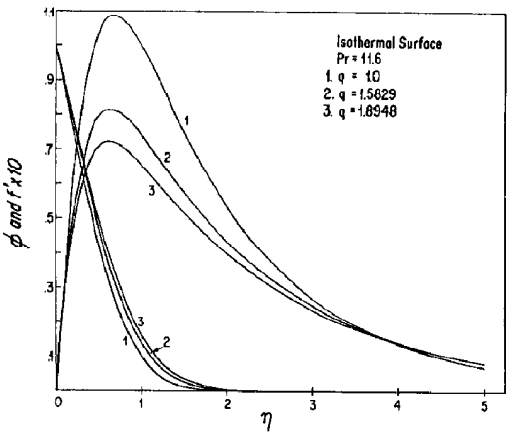

FIG. 7. Distributions of base flow velocity f' and temperature ϕ across the boundary region for an isothermal surface, $t_\infty = t_m$.

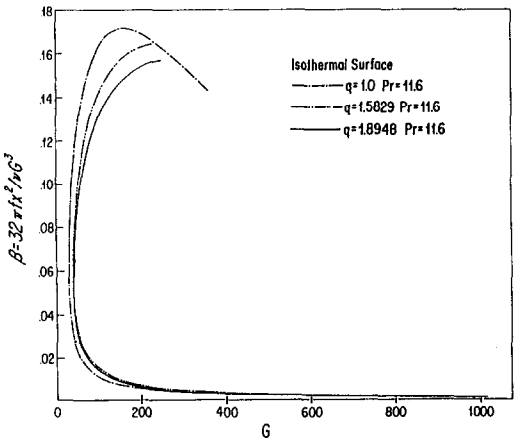

FIG. 8. Neutral stability curves for an isothermal surface.

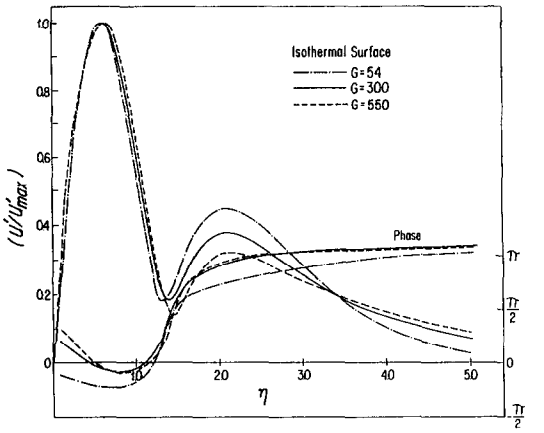

FIG. 10. u'/u'_{max} and phase distributions for an isothermal surface along a path $B = 0.36$, $q = 1.8948$.

velocity, normalized by a function of Grashof number, which in turn contains q. Even so, the density extremum weakens the buoyancy force and decreases the vigor of the flow.

In Fig. 3 neutral curves are compared, for $q = 1.0$, 1.5829 and 1.8948, for $Pr = 11.6$. The neutral curve for $q = 1.0$, $Pr = 6.7$, is also shown. At $Pr = 11.6$, the flow appears to be stabilized as the value of q increases. However, a comparison must be made in terms of physical quantities, such as the distance from the leading edge where a disturbance becomes neutrally stable, x_N. As an example, consider a surface dissipating 1000 W/m^2 in ambient water at 20°C and $q = 1$ and at 4°C and $q = 1.8948$. The downstream locations of first instability are $x_N = 2$ cm and 4.57 cm, respectively. Thus, the density anomaly has stabilized the flow.

The effects at different pressure levels may be estimated in the same way. At a given salinity, the value of $q(s,p)$ decreases with increasing pressure. Therefore, x_N increases slightly with pressure. However, at a given pressure, the variation of $q(s,p)$ with salinity is not monotonic.

The amplification contours for $q = 1.8948$, and for $Pr = 11.6$, and for $q = 1$ and $Pr = 6.7$, are plotted in Fig. 4. For $q = 1.8948$ the flow is more stable in these coordinates initially. However, downstream, as G increases, the rate of disturbance amplification becomes much faster. That is, equal A contours are crossed more quickly. The first downstream appearance of temperature and velocity disturbances in the experimental study [11] were at values of G at which $A = 6$–10 on Fig. 4. For a flux level of 1000 W/m^2 the downstream location x, for $A = 6$, are 44 cm and 39 cm for $q = 1.8948$ and 1.0, respectively. For $A = 9$, the downstream location is the same. That is, the amplification has been the same.

The paths of different physical frequencies in Figs. 4(a–d) indicate that a particular band of frequency components are selectively amplified. The most amplified frequency in this band is called the characteristic disturbance frequency. Gebhart and Mahajan [14] give the characteristic frequencies from the past calculations and experimental studies in water and air.

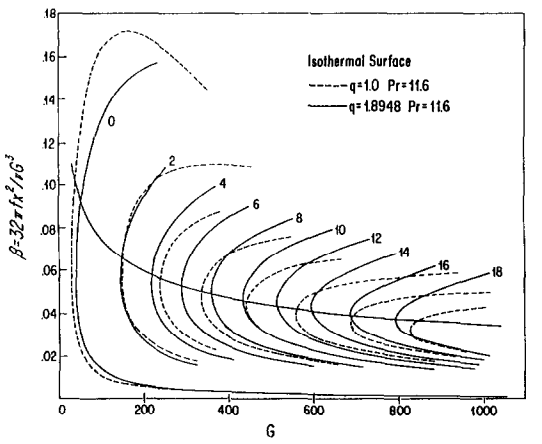

FIG. 9. Amplification rate contours for an isothermal surface.

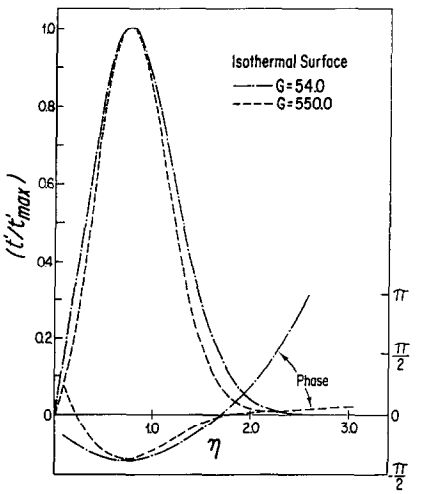

FIG. 11. t'/t'_{max} and phase distributions for an isothermal surface along a path $B = 0.36$, $q = 1.8948$.

For water, at room temperature, $Pr = 6.7$, the resulting frequency parameter is 0.675, for a uniform surface flux. Using the general formulation, equation (23), this value is $B^* = 0.731$. This is based on the frequency path in Fig. 4 which passes through the minimum G values attained by the contours $A = 6$ and 10, for $q = 1.0$.

However, for $q = 1.8948$, one particular frequency path does not pass through these minimum G values. Instead the value of B^* there increases with A. The disturbance frequencies measured in cold water, $t_\infty = 4°C$, by Qureshi and Gebhart [11] are shown in Fig. 4. Over the range of $A = 6$ to 12, the value of B^* at the minimum G location varies from 1.32 to 1.51. Thus, the experiments confirm both these stability calculations and this trend in downstream frequency modification.

Thus, the value of the characteristic frequency B^* changes from 0.731 to 1.512 as the ambient water temperature changes from 20 to 4°C. Since the definition of B^* as given by equation (23) contains the parameter q, it does not explicitly indicate the effect of ambient temperature level on the physical frequency. The actual effect is seen by calculating the frequency f for a surface dissipating 1000 W/m^2 in 20 and 4°C ambient water. The values are 0.2 Hz and about 0.12 Hz. Thus, in addition to stabilizing the flow, the colder ambient medium decreases the value of the predominant physical frequency.

Calculated eigenfunctions are plotted in their normalized forms, for comparisons with data. Figure 5 shows the distributions of u'/u'_{max} and the phase angle change, across the boundary region, along the path C in Fig. 4. The three distributions shown apply for three downstream locations $G = 90$, on the neutral curve, and at $G = 350$ and 550. The disturbance level at the outer edge of the velocity boundary layer increased downstream. The inner peak occurs around $\eta = 0.6$. The disturbance temperature distributions, t'/t'_{max}, along with their phase angle variation, are shown in Fig. 6, at $G = 90$ and 550. The major difference is in phase distribution. The data from [11] are also shown in Figs. 5 and 6. For both u' and t', excellent agreement is found near the surface. The disagreement for $\eta > 1.5$ in Fig. 5 arises both because the velocities are both low and comparable to the large horizontal entrainment effect there.

The isothermal condition

The base flow, stability and disturbance growth characteristics for this condition were also determined. Figure 7 compares the base flow velocity and temperature distributions across the boundary layer for $q = 1.0$, 1.5829 and 1.8948, for $Pr = 11.6$. Again the extremum effect is to decrease the buoyancy and hence the velocity levels.

The neutral curves, for increasing values of $q(s,p)$, in Fig. 8, again show that the flow is initially more stable. To maintain same $\Delta t = t_o - t_\infty$ in cold water, less heat flux is required because of the low velocity level, compared with that at $t_\infty = 20°C$. This stabilizes the flow. The effects of pressure and salinity levels on stability are the same as found for the uniform flux conditions.

The amplification contours for $q = 1.8948$ and 1.0, in Fig. 9, again indicate initial stabilization. However, downstream disturbance amplification rates become greater. For $q = 1.8948$, a single constant frequency path, $B = 0.36$, passes almost exactly through all of the minimum G values, across the whole range from 6 to 14. Recall that, for uniform flux, the characteristic frequency varies downstream. The value, $B = 0.36$, also was found to apply for $q = 1.5829$, 1.8364 and 1.8632.

The value of B is 0.25 for flows arising in warm ambient, $q = 1.0$, see Ref. [14]. Again, to determine the effect of lowering the ambient temperature on the predominant physical frequency f is calculated from equation (22). For an isothermal surface maintained 8°C above the ambient temperature, the predominant physical frequency is 0.3 Hz when $t_\infty = 20°C$ and 0.15 Hz when $t_\infty = 4°C$. This trend is consistent with that for a uniform flux condition. The distributions of u'/u'_{max} and t'/t'_{max} are shown in Figs. 10 and 11, for different values of G along the path $B = 0.36$. The corresponding phase angle distributions are also shown. These results are very similar to those found for the flux condition.

6. CONCLUSIONS

The calculations for the flux and temperature conditions show that a tendency toward a density extremum has considerable effects both on initial laminar instability and on downstream disturbance growth. The effects for the two surface conditions are very similar. In cold water, the buoyancy is reduced and the flow is more stable. The downstream rate of disturbance growth is also less, in physical terms. However, the same kind of sharply selective disturbance amplification mechanisms arise. A narrow band of a general disturbance spectrum is still amplified much more rapidly. The central or characteristic frequency again remains approximately constant downstream. However, its value is reduced almost by a factor of two compared with the predominant frequency found in warmer ambient medium. Data for both the characteristic frequency and the disturbance amplitudes, are in excellent agreement with the results of these calculations.

Acknowledgement—The authors wish to acknowledge support for this study by the National Science Foundation under Grant MEA 82 17756.

REFERENCES

1. B. Gebhart and R. L. Mahajan, Instability and transition in buoyancy induced flows, *Adv. appl. Mech.* **22**, 231–315 (1982).
2. M. S. Bendell and B. Gebhart. Heat transfer and ice

melting in ambient water near its density extremum, *Int. J. Heat Mass Transfer* **19,** 1081–1087 (1976).
3. B. Gebhart and J. C. Mollendorf, Buoyancy-induced flows in water under conditions in which density extrema may arise, *J. Fluid Mech.* **89,** 673–707 (1978).
4. V. P. Carey, B. Gebhart and J. C. Mollendorf, Buoyancy force reversals in vertical natural convection flows in cold water, *J. Fluid Mech.* **97,** 279–297 (1980).
5. I. El Henawy, B. Hassard, N. D. Kazarinoff, B. Gebhart and J. C. Mollendorf, Numerically computed multiple steady states of buoyancy induced flow in cold water, *J. Fluid Mech.* **122,** 235–250 (1982).
6. E. G. Josberger and S. Martin, Laminar and turbulent boundary layers adjacent to melting vertical ice walls in salt water, *J. Fluid Mech.* **111,** 439–473 (1981).
7. V. P. Carey and B. Gebhart, Visualization of flow adjacent to a vertical ice surface melting in cold pure water, *J. Fluid Mech.* **107,** 37–55 (1981).
8. V. P. Carey and B. Gebhart, Transport near a vertical ice surface melting in saline water, measurements at low salinity, *J. Fluid Mech.* **117,** 402–423 (1982).
9. J. M. Higgins and B. Gebhart, The stability of vertical buoyancy induced flow in cold water, *J. Heat Transfer* **105,** 767–773 (1983).
10. J. M. Higgins and B. Gebhart, Measurements of instability and disturbance growth in vertical buoyancy induced flows in cold water, *Int. J. Heat Mass Transfer* **25,** 1397–1409 (1982).
11. Z. H. Qureshi and B. Gebhart, Measurements of fluid and thermal transport in vertical buoyancy induced flows in cold water, *Int. J. Heat Mass Transfer* **24,** 1503–1511 (1981).
12. B. Gebhart and J. C. Mollendorf, A new density relation for pure and saline water, *Deep-Sea Res.* **24,** 831–848 (1977).
13. C. A. Hieber and B. Gebhart, Stability of vertical natural convection boundary layers: some numerical solutions, *J. Fluid Mech.* **48,** 625–646 (1971).
14. B. Gebhart and R. L. Mahajan, Characteristic disturbance frequency in vertical natural convection flow, *Int. J. Heat Mass Transfer* **18,** 1143–1148 (1975).

LA STABILITE DES ECOULEMENTS NATURELS THERMIQUES VERTICAUX DANS L'EAU PURE ET L'EAU SALEE

Résumé—Des mouvements naturels se forment couramment dans l'eau pure et l'eau salée. L'anomalie de densité de l'eau à 4°C et à la pression atmosphérique a des effets importants sur le mouvement. On étudie les mécanismes pour différentes géométries et conditions, principalement pour l'écoulement laminaire. Cette étude précise la stabilité des écoulements adjacents à une paroi verticale, soumise à un flux uniforme ou à température constante, pour l'eau pure à deux niveaux de pression. La condition spécifique traitée est celle d'un milieu ambiant au repos et pour la condition relativement faible, la variation de densité à travers la couche limite a des effets importants sur l'instabilité et sur la croissance des perturbations en aval. Les résultats nouveaux obtenus sont comparés avec des mesures récentes du comportement de perturbation et cela avec un accord excellent.

DIE STABILITÄT VON THERMISCHEN AUFTRIEBSSTRÖMUNGEN IN KALTEM REINEM UND MIT SALZ VERSETZTEM WASSER

Zusammenfassung—Strömungen aufgrund von Dichteunterschieden in reinem und salzigem kaltem Wasser treten häufig auf. Die Dichteanomalie des Wassers mit dem Maximum bei etwa 4°C in reinem Wasser bei Umgebungsdruck beeinflußt Strömungs- und Transportvorgänge stark. Die daraus entstehenden Vorgänge wurden für verschiedene Anordnungen und Bedingungen untersucht, in erster Linie bei laminarer Strömung. Die vorliegende Studie untersucht Stabilitäts- und Instabilitätserscheinungen von Anlaufströmungen entlang senkrechter Oberflächen in reinem Wasser bei zwei Drücken, sowohl bei isothermer Randbedingung als auch bei konstanter Wärmestromdichte. Insbesondere wird jener Bereich untersucht, bei dem das ruhende Medium gerade das Dichtemaximum aufweist. Es stellt sich heraus, daß selbst dieser relativ geringe Dichteunterschied in der thermischen Grenzschicht bis hin zum Dichtemaximum das Entstehen der Instabilität und das Anwachsen von Störungen erheblich beeinflußt. Die Art der Instabilitäten und ihre selektive Verstärkung ist allerdings ähnlich wie bei normaleren Fluidzuständen. Die hier berichteten neuen Ergebnisse wurden mit kürzlich durchgeführten Messungen des Störungsverhaltens verglichen, es wurde sehr gute Übereinstimmung festgestellt.

УСТОЙЧИВОСТЬ ИНДУЦИРУЕМЫХ ПОДЪЕМНОЙ СИЛОЙ ВЕРТИКАЛЬНЫХ ПОТОКОВ В ХОЛОДНОЙ ЧИСТОЙ И СОЛЕНОЙ ВОДЕ

Аннотация -Индуцируемые подъемной силой потоки в холодной чистой и соленой воде представляют обычное явление. Аномальное поведение плотности холодной воды, например, ее экстремум приблизительно при 4°C в чистой воде при атмосферном давлении, обычно сильно влияет на характер течения и перенос. Механизм действия подъемной силы изучался для различных геометрий и граничных условий, главным образом для ламинарного потока. В данной работе для двух уровней давления исследуются механизмы устойчивости и неустойчивости развивающихся в чистой воде течений вблизи вертикальной поверхности для однородного потока и изотермических граничных условий. Рассмотрен случай, когда плотность неподвижной окружающей среды является экстремальной. Обнаружено, что даже относительно слабое возрастание плотности поперек теплового слоя в жидкости до экстремального значения сильно влияет на развитие устойчивости возмущений вниз по потоку. Однако характер неустойчивостей и их избирательное усиление качественно такие же, как и при обычных условиях. Сравнение полученных новых результатов с недавно проведенными измерениями показывает их прекрасное согласие.